Frequency-chirped subwavelength nanoantennas

Ami Yaacobi* and Michael R. Watts

Photonic Microsystems Group, Research Laboratory of Electronics, Massachusetts Institute of Technology, 77 Massachusetts Ave., Cambridge, Massachusetts 02139, USA

**Corresponding author: amiya@mit.edu*

Received September 12, 2012; revised November 5, 2012; accepted November 5, 2012; posted November 6, 2012 (Doc. ID 175995); published November 30, 2012

Herein we propose, theoretically investigate, and numerically demonstrate the first use to our knowledge of frequency chirping to achieve broadband, efficient subwavelength vertical emission from a dielectric waveguide. We demonstrate this unique and effective approach in the telecom C band in a nanophotonic frequency-chirped dipole antenna. The structure utilizes a plasmonic antenna placed above an Si_3N_4 waveguide and a ground plane to enhance emission efficiency. Three-dimensional finite-difference time-domain simulations reveal up to 55% vertical emission efficiency, and a bandwidth of 500 nm is possible in a structure less than half a wavelength long. The design methodology and theoretical underpinnings of frequency-chirped nanophotonic antennas coupled to dielectric waveguides are presented.

OCIS codes: 250.5403, 130.0130, 060.1810.

Vertical coupling can be used in silicon-on-insulator-based optical phased arrays (OPAs) for the purpose of emitting light traveling in a waveguide to a free-space mode [1,2]. Vertical input/output coupling has previously been extensively investigated for the purpose of coupling to or from an optical fiber [3–7], but, as a result, most vertical couplers to date have emission patterns matched to fiber modal diameters (~10 μm) and size of the same order or larger. In an OPA, however, the desired emitter characteristics include strong waveguide-to-free-space output coupling in a compact structure—ideally less than one wavelength long. A short emitter length is critical to fitting many emitters in a small area and to enabling wide divergence angles within a single lobe. However, demonstrations of efficient output coupling using short structures are uncommon; minimum structure lengths found to be several wavelengths long [5,7,8]. Short emitters have also been demonstrated using nanoantenna designs translated from the RF to optical bands [8–11], but traditional RF antennas differ from photonic nanoantennas in at least one important way: RF antennas are fed from thin transmission lines, enabling the excitation of the antenna to occur from a single location. In a photonic nanoantenna, the open dielectric waveguide precludes separation of the guided wave from the antenna structure, and the guided wave interacts with the entire antenna. This fundamental difference suggests that a different tact should be taken to enable compact and efficient emission from antennas coupled to dielectric nanophotonic waveguides.

We propose and numerically demonstrate the use of deep subwavelength frequency-chirped elements to enable subwavelength emission from a nanophotonic dielectric waveguide. Finite-difference time-domain (FDTD) simulations of a one-layer antenna plus a ground plane show 55% up emission with a structure only one third of a free-space wavelength long. The antenna is a cluster of metallic nanorods designed to work in the C band; however, the results here are general and can be applied to any chirped structure and any band of the electromagnetic spectrum to achieve efficient, subwavelength coupling between two propagating modes.

To gain intuition about the coupling between the nanoantenna and the waveguide, we treat the nanoantenna as a resonator and use coupled-mode theory in the time domain [12–14]. Coupled-mode theory assumes shape invariance of the modes and drops second-order terms, enabling quantitatively accurate results only with weakly coupled modes; however, it provides useful qualitative insight even when modes are strongly coupled.

The differential equation governing the reaction of a resonator with energy amplitude a and coupling coefficient μ to a perturbing mechanism (e.g., a waveguide) with field amplitude s is, to the first order [12],

$$\frac{d}{dt}a = \left(j\omega_0 - \frac{1}{\tau}\right)a - j\mu s, \tag{1}$$

where ω_0 is the resonance frequency and τ is its field decay rate. In a nanophotonic antenna, the loss mechanisms can be broken down into radiation, ohmic, and coupling losses, with decay rates τ_r, τ_o, and τ_e, respectively. The steady-state solution to Eq. (1) with input s at frequency ω is

$$a = \frac{-j\mu s}{j(\omega - \omega_0) + 1/\tau} \equiv sRe^{j\Delta\varphi}, \tag{2}$$

where we define the resonator response to have amplitude R and phase $\Delta\varphi$. It is easy to see that one can change the phase response of the resonator, $\Delta\varphi$, through a maximum total range of π radians. When μ is positive, $\Delta\varphi$ will vary in the range $(-\pi, 0)$, depending on the value of ω_0. If the resonator mode is leaky, the phase of the emitted field will be the same as that of the resonator.

Using this principle and the space dependence of the input wave, $\exp(-j\vec{k}z)$, we can place several resonators with different resonances along the waveguide in such a way that they all resonate with the same phase. Thus, the resonators will constructively interfere to form a vertically emitted wave. As Fig. 1(a) shows, a single dipole driven by a plane wave emits in all directions. However, a set of frequency-chirped dipoles can be combined to interfere and form a flatter wavefront and larger antenna gain as shown in Fig. 1(b), enabling efficient vertical

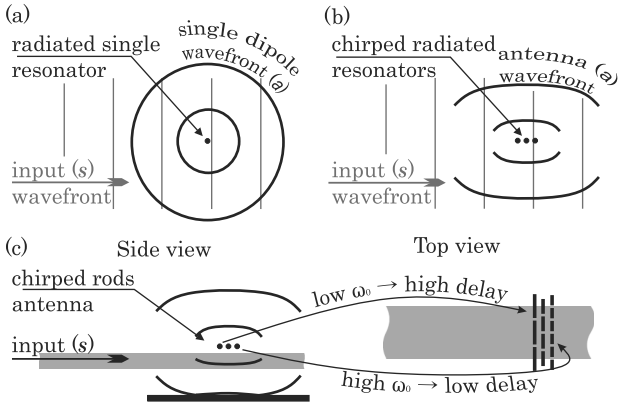

Fig. 1. (a) Side view of a single resonator (here a dipole) driven by a plane wavefront, (b) a set of chirped resonators design for right-angle wave coupling driven with the same source as (a), and (c) side and top view of a set of resonators designed for vertical coupling from a waveguide to free space. Total structure length is smaller than $\lambda/2n_{\text{eff}}$.

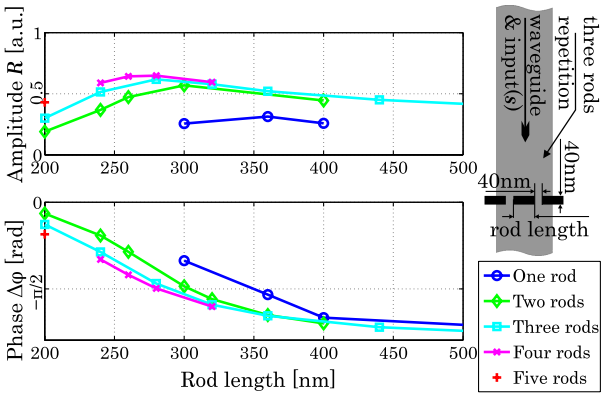

Fig. 2. (Color online) Amplitude R (top) and phase $\Delta\varphi$ (bottom) versus rod length for lateral repetition of specified number of rods and wavelength of 1550 nm (a three-rod example is shown on the right).

coupling. By additionally repeating the dipoles laterally, we further enhance the coupling at each longitudinal position. The resulting antenna structure is illustrated in Fig. 1(c).

Considering cross talk between the different components of the antenna, we can rewrite Eq. (1) for a group of resonators a_i:

$$\frac{da_i}{dt} = \left(j\omega_i - \frac{1}{\tau_i}\right)a_i - j\sum_k \mu_{ik}a_k, \tag{3}$$

where ω_i and τ_i are the ith resonator natural resonance and decay rate, respectively, and μ_{ik} is the coupling coefficient from the kth to the ith resonator. It can be seen from Eq. (3) that, when all the resonators have same phase, no amplitude fluctuations are produced; there is only a redshift in the resonant frequency.

In this Letter, we use dipole rod resonators, with a dimension along the input $\vec{k}$ vector much shorter than a wavelength. We arrange several of these dipoles in a half-wavelength section (π phase region) to create a subwavelength coupler through constructive interference. Figure 1(c) illustrates the principle behind the structure of the vertical coupler. The specific vertical coupler designs presented here are based on frequency-chirped rod resonators placed in a plane above a Si_3N_4 waveguide. An additional metallic ground plane is placed under that waveguide to facilitate vertical coupling [see Fig. 1(c)]. For an example structure, we chose the following: (1) an 80 nm Al ground plane, (2) a 60 nm Al antenna layer, (3) an Si_3N_4 waveguide with a width of 700 nm and a 220 nm height, (4) a ground-plane-to-antenna separation of 680 nm, and (5) a waveguide-to-antenna separation of 100 nm. The permittivities of Si_3N_4 and SiO_2, are 4 and 2.1, respectively, at 1550 nm [15]. The Drude parameters used for aluminum were $\gamma_d = 2.4 \times 10^{14}$ rad/s and $\omega_p = 2.2 \times 10^{16}$ rad/s.

To design the antenna, the phase responses of dipole antennas of different lengths are examined. The responses are calculated via three-dimensional (3D) FDTD simulations using a waveguide with no ground plane as the feeding mechanism. The one-rod curve (blue) in Fig. 2 shows the resulting amplitude and phase responses at a wavelength of 1550 nm as a function of rod length. Using Eq. (2) and the asymptotic value of the phase response for the lowest resonance (about –2.5 rad), we calculate τ to be ~1 fs. With such a short decay intrinsic to a nanorod, each nanorod is inherently undercoupled. Thus, following [8], lateral repetition of the nanorods is needed to enhance overall coupling. Various sets of laterally repeated rods (same length in each set) were examined to determine their phase responses. Figure 2 shows the resulting responses as a function of rod length and repetition number. It can be seen that the maximum amplitude response always corresponds to the $-\pi/2$ phase response, as expected from Eq. (2).

Next we choose resonators with different phase responses and place them along the waveguide axis such that the sum of the input wave phase $\vec{k}_z$ and the specific phase response is same for all resonators. This results in constructive interference in the designed output direction. Finally, a correction to the rod length is made in order to correct for the redshift caused by the proximity of different resonators with the same phase.

Figure 3(a) compares the up emission of one four-rod set on resonance (blue solid curve) with the uncorrected (green dashed curve) and redshift-corrected (magenta dotted–dashed curve) frequency-chirped antennas. The rods in the uncorrected structure are arranged in sets 3×680 nm, 3×360 nm, 4×280 nm, 4×240 nm and 5×200 nm, where $A \times B$ nm stands for (repetition number) × (rod length in nm) and the order of writing is the order along the z axis. The corrected (blue-shifted) antenna has rods arranged in sets 3×630 nm, 3×320 nm, 4×240 nm, 4×200 nm, 5×160 nm and an extra 2×160 nm set. The solid black curve shows the ohmic losses to be under 10%. In order to obtain the results in Fig. 3(a), we monitored the spectral content of the fields over the surface of a box enclosing the structure. From this, we calculated the amount of energy leaving each facet [Fig. 3(b)]. All other losses, including emission out through the sides, bottom, and rear of the box, had significantly lower values (<10% each at 1550 nm). All cases depicted in Fig. 3 include a ground plane at a distance of $d \sim 3\lambda/4n$ for constructive vertical coupling. This

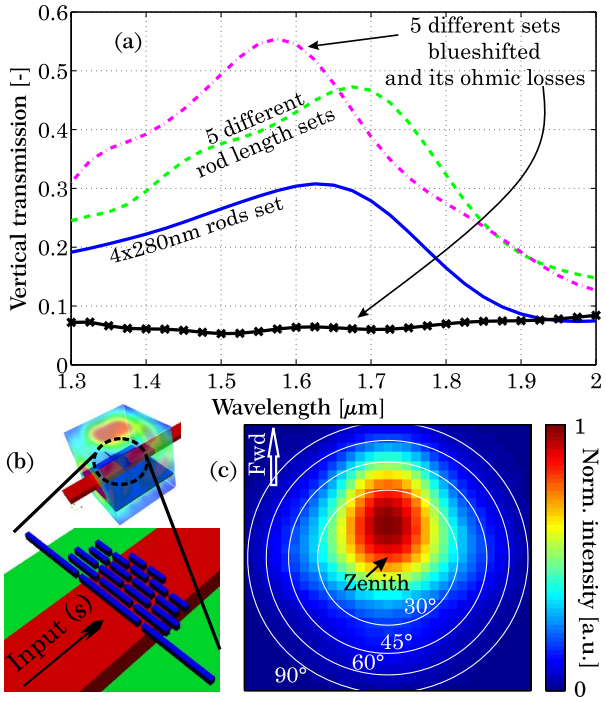

Fig. 3. (Color online) (a) Simulated vertical emission for different structures, each with a ground plane and (b) final structure with the time-integrated field box around it. (c) Free-space far-field pattern of the same structure at $\lambda = 1550$ nm.

was done so as to combine the bottom and top emission and maximize the vertical coupling. In total, we found 55% vertical emission, revealing efficient emission from a subwavelength structure. Additionally, as shown in Fig. 3(c), the main lobe from the full structure has less than a 30 deg FWHM, and therefore the output can be directed. Finally, the resulting bandwidth of a short (rapidly coupled) emitter goes up to ~500 nm.

In conclusion, by using 3D FDTD simulations, we show that metallic nanoantenna structures can vertically emit at least 55% of an input wave over a 3 dB bandwidth of 500 nm in a structure only one third of a free-space wavelength long. Furthermore, the proposed structure uses realistic dimensions and commonly available materials. By repeating the structure longitudinally, even more efficient emission could be produced. While efficient all-dielectric emitters have been demonstrated [1–5], to our knowledge this is the first proposed and numerically verified compact (less than a wavelength long) emitter design and the first proposed structure of its kind.

This work is supported by the DARPA Microsystems Technology Office (MTO) SWEEPER Project DE-AC04-94AL85000. We would like to thank Cheryl Sorace-Agaskar and Erman Timurdogan of MIT, Paul Davids and Rohan Kekatpure of Sandia, Nader Engheta of University of Pennsylvania, and Carmel Rotschild of Technion for helpful discussions.

References

1. K. V. Acoleyen, H. Rogier, and R. Baets, Opt. Express **18**, 13655 (2010).
2. J. K. Doylend, M. J. R. Heck, J. T. Bovington, J. D. Peters, L. A. Coldren, and J. E. Bowers, Opt. Express **19**, 21595 (2011).
3. G. Roelkens, D. Vermeulen, S. Selvaraja, R. Halir, W. Bogaerts, and D. V. Thourhout, IEEE J. Sel. Top. Quantum Electron. **17**, 571 (2011).
4. M. Fan, M. A. Popović, and F. X. Kärtner, in *Conference on Lasers and Electro-Optics/Quantum Electronics and Laser Science Conference and Photonic Applications Systems Technologies*, OSA Technical Digest Series (CD) (Optical Society of America, 2007), paper CTuDD3.
5. B. Wang, J. Jiang, and G. P. Nordin, IEEE Photonics. Technol. Lett. **17**, 1884 (2005).
6. K. Kintaka, Y. Kita, K. Shimizu, H. Matsuoka, S. Ura, and J. Nishii, Opt. Lett. **35**, 1989 (2010).
7. G. Roelkens, D. V. Thourhout, and R. Baets, Opt. Lett. **32**, 1495 (2007).
8. A. Yaacobi, E. Timurdogan, and M. Watts, Opt. Lett. **37**, 1454 (2012).
9. D. Dregely, R. Taubert, J. Dorfmuller, R. Vogelgesang, K. Kern, and H. Giessen, Nat. Commun. **2**, 267 (2011).
10. T. Kosako, Y. Kadoya, and H. F. Hofmann, Nat. Photonics **4**, 312 (2010).
11. J. Li and N. Engheta, IEEE Trans. Antennas Propag. **55**, 3018 (2007).
12. B. E. Little, S. T. Chu, H. A. Haus, J. Foresi, and J. P. Laine, J. Lightwave Technol. **15**, 998 (1997).
13. H. A. Haus, in *Waves and Fields in Optoelectronics* (Prentice-Hall, 1984), pp. 197–207.
14. H. A. Haus and W. P. Huang, Proc. IEEE **79**, 1505 (1991).
15. H. R. Philipp, in *Handbook of Opt. Const. of Solids*, E. D. Palik, ed. (Elsevier, 1998), pp. 760–774.